Doubly stochastic enhancement of the Failure Forecast Method using a noisy mean-reverting process and application to volcanic eruption forecasts

Andrea Bevilacqua[1], E. Bruce Pitman[2], Abani K. Patra[3,4], and Augusto Neri[5]

[1]*Dept. of Earth Sciences, University at Buffalo, Buffalo, NY*
[2]*Dept. of Materials Design and Innovation, University at Buffalo, NY*
[3]*Dept. of Mech. and Aero. Eng., University at Buffalo, Buffalo, NY*
[4]*Comp. Data Science and Eng., University at Buffalo, Buffalo, NY*
[5]*Sezione di Pisa, Istituto Nazionale di Geofisica e Vulcanologia, Pisa, Italy*

`{abevilac,pitman,abani}@buffalo.edu; augusto.neri@ingv.it`

Abstract

We introduce a doubly stochastic method for performing material failure theory based forecasts of volcanic eruptions. The method enhances the well known Failure Forecast Method equation, introducing a new formulation similar to the Hull-White model in financial mathematics. In particular, we incorporate a stochastic noise term in the original equation, and systematically characterize the uncertainty. The model is a stochastic differential equation (SDE) with mean reverting paths, where the traditional ordinary differential equation (ODE) defines the mean solution. Our implementation allows the model to make excursions from the classical solutions, by including uncertainty in the estimation. The doubly stochastic formulation is particularly powerful, in that it provides a complete posterior probability distribution, allowing civil protection officials to determine a worst case scenario with a specified level of confidence. We validate the new method on historical datasets of precursory signals, across a wide range of possible values of convexity in the solutions and amounts of scattering in the observations. The results show the increased forecasting skill of the doubly stochastic formulation of the SDE.

1 Introduction

The Failure Forecast Method (FFM) for volcanic eruptions is a classical tool in the interpretation of monitoring data as potential precursors, providing quantitative predictions of the eruption onset. The basis of FFM is a fundamental law for failing materials:

$$dX/dt = AX^\alpha,$$

where X is the rate of the precursor signal, and α, A are model parameters. The solution X is a power law of exponent $1/(1 - \alpha)$ diverging at time t_f, called failure time. The model represents the potential cascading of precursory signals leading to the final rupture of materials, with t_f a good approximation to the eruption onset time t_e.

The FFM equation was originally developed in landslide forecasting (Fukuzuno, 1985; Voight, 1987, 1988b; Voight et al., 1989), and later applied in eruption forecasting (Voight, 1988a, 1989; Cornelius and Voight, 1995). The method was retrospectively applied to several volcanic systems, including dome growth episodes and explosive volcanic eruptions (Voight and Cornelius, 1991; Cornelius and Voight, 1994, 1996; Voight et al., 2000).

Seismic data are the type of signals most extensively studied with the FFM method in volcanology. Volcanic tremor has been related to the multi-scale rock cracking (Kilburn and Voight, 1998; Ortiz et al., 2003; Kilburn, 2003; Smith et al., 2009) and volcano-tectonic earthquakes can be forecasted applying the FFM on its characteristics (Tárraga et al., 2006). Rheological experiments on lava domes revealed that also the magma seismicity is consistent with the FFM theory (Lavallée et al., 2008). In general, retrospective analysis of pre-eruptive seismic data produced good results in several case studies (e.g. Smith and Kilburn (2010); Budi-Santoso et al. (2013); Chardot et al. (2013)). Finally, the FFM has been successfully tested on Synthetic Aperture Radar acquisitions, opening the path to new forecasting applications based on satellite data (Moretto et al., 2016).

The reliability of FFM forecasts is known to be affected by several factors. When applied to seismic data, the performance of the method is usually higher on eruptions preceded by a single phase of seismic acceleration (Boué et al., 2015). The preliminary separation of signals originating from different sources can improve the results (Salvage and Neuberg, 2016; Salvage et al., 2017). Technically, nonlinear (power law) regression or non-Gaussian maximum likelihood methods can also enhance the accuracy of the forecasts, compared to linear models (Bell et al., 2011, 2013). In general, the forecasting accuracy of FFM has been related to the heterogeneity in the breaking material (Vasseur et al., 2015). However, sometimes the method fails to predict the time of material failure, and some volcanic systems are often characterized by prolonged unrest and ambiguous signals (Chiodini et al., 2016). A full probability assessment, including uncertainty quantification (UQ), is required, and it is the purpose of our investigations.

In this study, we generalize the classical FFM approach by incorporating a stochastic noise in the original ordinary differential equation (ODE), converting it into a stochastic differential equation (SDE), and systematically characterizing the uncertainty. Embedding noise in the model can enable the FFM equation to have greater forecasting skill by focusing on averages and moments. Sudden changes in the power law properties are made possible. In our model, the prediction is thus perturbed inside a range that can be tuned, producing probabilistic forecasts.

In more detail, in the original equation the change of variables $\eta = X^{1-\alpha}$ implies:

$$d\eta/dt = (1 - \alpha)A,$$

i.e. a straight line which hits zero at t_f. The most efficient graphical and computational methods indeed rely on the regression analysis of inverse rate plots. We re-define η with:

$$d\eta_t = \gamma[(1 - \alpha)A(t - t_0) + \eta_{t_0} - \eta_t]dt + \sigma dWt,$$

also called Hull-White model in financial mathematics (Hull and White, 1990). The parameter σ defines the strength of the noise, and γ the rapidity of the mean-reversion property. We validate the new method on historical datasets of precursory signals already studied with the classical FFM, including line-length and fault movement at Mt. St. Helens, 1981-82, seismic signals registered from Bezymyanny, 1960, and surface movement of Mt. Toc, 1963 (Voight, 1988a).

A fundamental aspect of our formulation is the possibility of a doubly stochastic UQ. Doubly stochastic models describe the effect of uncertainty in the formulation of aleatory processes, and have been successfully applied in volcanology (Sparks and Aspinall, 2004; Marzocchi and Bebbington, 2012; Bevilacqua, 2016). Thus, doubly stochastic probability density functions (pdf) and estimates are themselves affected by uncertainty. This approach has been applied in spatial problems concerning eruptive vent/fissure mapping (Selva et al., 2012; Bevilacqua et al., 2015; Tadini et al., 2017b,a; Bevilacqua et al., 2017a), long-term temporal problems based on past eruption record (Bebbington, 2013; Bevilacqua et al., 2016; Richardson et al., 2017; Bevilacqua et al., 2018), and hazard assessments (Neri et al., 2015; Bevilacqua et al., 2017b). In this study, we use a doubly stochastic model to develop a short-term eruption forecasting method based on precursory signals.

The first part of this article defines the mathematical model adopted. In section 2 we present the equations in FFM method, in section 3 we define their enhancement with a mean-reverting SDE, and section 4 details the properties of the mean reversion. The second part of the article tests the model on historical datasets. In section 5 we define the fitting algorithm and compare retrospective analysis based on three different formulations of FFM. Section 6 tests the model on forecasting problems, and section 7 discusses the performance of the methods, showing the increased forecasting skill of the doubly stochastic formulation.

2 The Failure Forecast Method ODE

The classical Failure Forecast Method (FFM) equation is:

$$\dot{\Omega}^{-\alpha}\ddot{\Omega} = A, \tag{1}$$

where $\alpha \geq 1$, $A > 0$, and $\Omega : [0, T] \to \mathbb{R}$ a precursor function, like ground or fault displacement, seismic strain release (Voight, 1988a). For simplicity we call $X := \dot{\Omega}$, and the equation 1 reads:

$$X^{-\alpha}\frac{dX}{dt} = A.$$

If $\alpha = 1$, the solution is the exponential $X(t) = X(t_0)\exp[A(t - t_0)]$. However, most common observations in volcanology give $\alpha \in [1.7, 2.3]$. We note that if $\alpha < 1$ a solution exists in $[0, +\infty]$ and does not diverge in a finite time (Cornelius and Voight, 1995).

If $\alpha > 1$, we see:

$$\frac{dX^{1-\alpha}}{dt} = (1-\alpha)X^{-\alpha}\frac{dX}{dt},$$

and the FFM equation becomes:

$$\frac{dX^{1-\alpha}}{dt} = (1-\alpha)A.$$

Simplifying again the notation, we can call $\eta = X^{1-\alpha}$, and the FFM reads:

$$\frac{d\eta}{dt} = (1-\alpha)A.$$

We can solve this equation by immediate integration,

$$\eta(t) = (1-\alpha)A(t-t_0) + \eta(t_0), \tag{2}$$

and equivalently:

$$X(t) = \left[(1-\alpha)A(t-t_0) + X(t_0)^{1-\alpha}\right]^{\frac{1}{1-\alpha}}. \tag{3}$$

The original method required fitting the two parameters α and A on the monitoring data, and then to estimate the time of failure t_f, such that $X(t_f) = +\infty$, or equivalently $\eta(t_f) = 0$. It follows:

$$t_f = \inf\{t : \eta(t) = 0\}, \qquad \eta(t) = (\alpha - 1)A(t_f - t),$$

and so:

$$t_f - t = \frac{\eta(t)}{(\alpha - 1)A}.$$

We note that an estimate of $\eta(t)$ is thus necessary to make forecasts, a non-trivial process if noise is assumed to be present. The effect of varying parameters α and A in the equation 3 is displayed in Figure 1a,b. Our purpose is to forecast the failure time t_f, and hence it is more practical to examine the plot of $X^{-1} = \eta^{\frac{1}{\alpha-1}}$, shown in Fig.1b. The parameter α defines the convexity of that function - for $\alpha \leq 2$ it is convex, for $\alpha \geq 2$ it is concave. The value $\alpha = 2$ produces a straight line. We call α the *convexity* parameter. In equation 2 the parameter A changes the time scale of the equation, and so defines the constant slope of η, that is $-A$. Hence we call A the *slope* parameter.

3 The Failure Forecast Method SDE

We assume that the equation is not exactly satisfied, but there is a transient difference, which however decreases exponentially through time. The equation becomes:

$$\eta(t) = (1-\alpha)A(t-t_0) + \beta\exp(-\gamma t) + \eta(t_0),$$

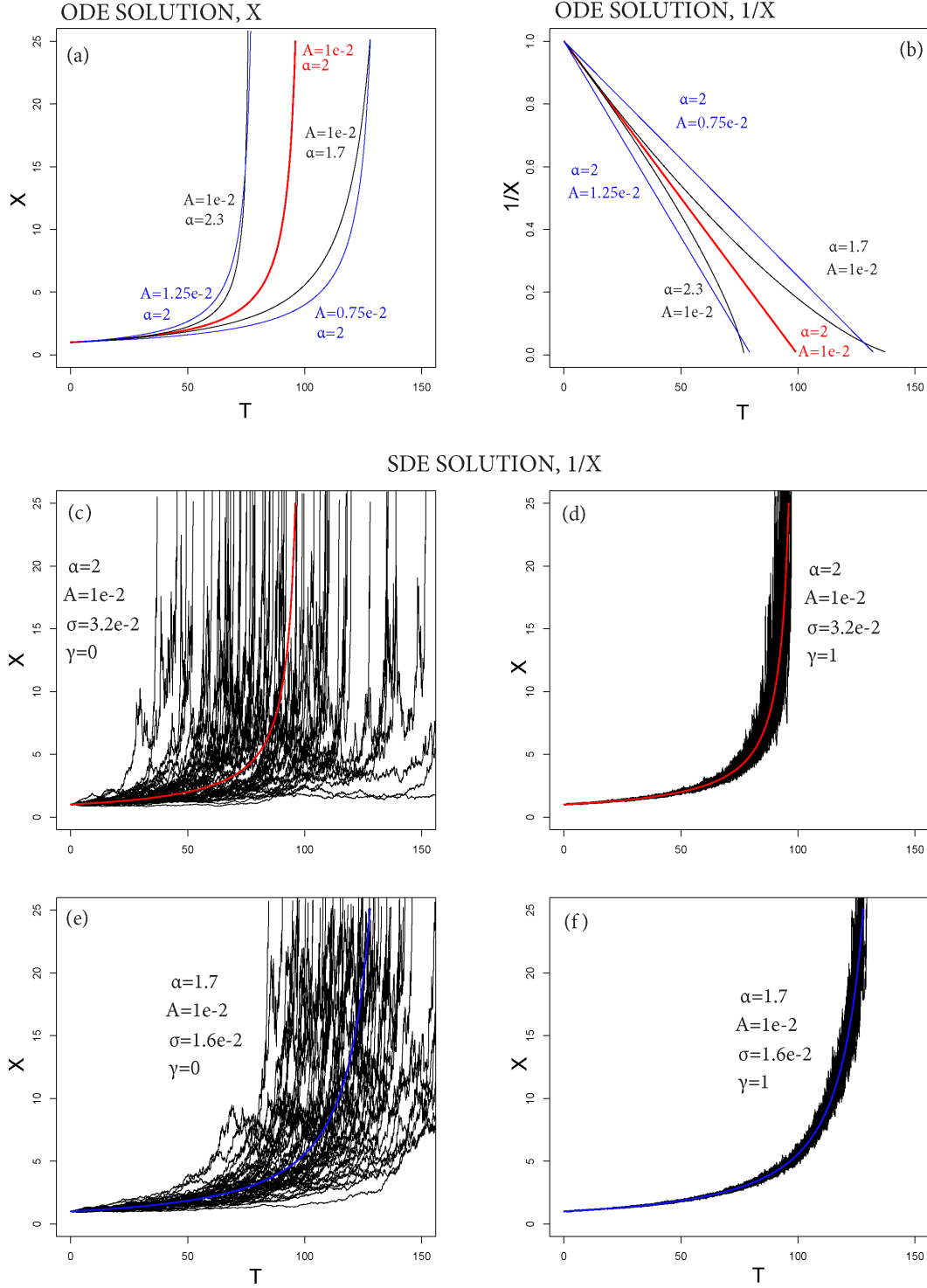where β is the value at $t = 0$ and γ is the rate of decay of this error term.

3

Figure 1: (a,b) ODE solution, (a) X, and (b) 1/X. (c-f) SDE solution, (c,e) with $\gamma = 0$, (d,f) with $\gamma = 1$. (c,d) with $\alpha = 2$, (e,f) with $\alpha = 1.7$. The colored lines are the ODE solutions, the black lines are 50 random paths of the SDE solutions.

4

This allows a reformulation of the equation. Given that:

$$\eta(t) - (1 - \alpha)A(t - t_0) - \eta(t_0) = \beta \exp(-\gamma t),$$

then

$$\ln\left[\eta(t) - (1 - \alpha)A(t - t_0) - \eta(t_0)\right] = -\gamma t + ln(\beta).$$

We can take the derivative, and obtain:

$$\left[\eta(t) - (1 - \alpha)A(t - t_0) - \eta(t_0)\right]^{-1}\left(\frac{d\eta}{dt}(t) - (1 - \alpha)A\right) = -\gamma,$$

and so

$$\frac{d\eta}{dt} = \gamma\left[(1 - \alpha)A(t - t_0) + \eta(t_0) - \eta(t)\right] + (1 - \alpha)A. \tag{4}$$

In addition, we want to allow for an additive noise affecting the new equation, and the final formulation is:

$$d\eta_t = \left\{\gamma\left[(1 - \alpha)A(t - t_0) + \eta_{t_0} - \eta_t\right] + (1 - \alpha)A\right\}dt + \sigma dW_t, \tag{5}$$

or equivalently:

$$X_t = \left\{X_{t_0}^{1-\alpha} + \int_{t_0}^{t}\left\{\gamma\left[(1 - \alpha)A(s - t_0) + X_{t_0}^{1-\alpha} - X_s^{1-\alpha}\right] + (1 - \alpha)A\right\}dt + \int_{t_0}^{t}\sigma dW_s\right\}^{\frac{1}{1-\alpha}}, \tag{6}$$

for each $t < t_f$. This is also called a Hull-White model in financial mathematics (Hull and White, 1990).

The effect of varying parameters σ and γ on the SDE solution X is displayed in Figure 1c-f. In equation 5, σ defines the time scale of the additive noise, and so we call σ the *noise* parameter. We remark that X is nonlinearly affected by this random noise in equation 6. The SDE defining η is elevated to the exponent $\frac{1}{1-\alpha}$, and even a relatively small noise can significantly change the failure time (see Fig.1c,e). Parameter γ defines the time scale of the exponential decay of perturbations with respect to the mean solution. It controls the equation, reverting the paths of the solutions towards the mean curve (see Fig.1d,f). We call γ the *mean-reversion* parameter.

The new formulation allows the SDE solution to make random excursions from the classical ODE solution. Figure 2 displays three different solutions of X^{-1}, assuming convexity parameter $\alpha = 1.7$, 2, or 2.3. The slope parameter is fixed $A = 0.1$. Plots 2a,c,e show an example of solutions assuming mean-reversion parameter $\gamma = 0$, or $\gamma = 0.25$. The noise is additive in 2a, and weakly nonlinear in 2c,e. We note that σ and γ define the noise affecting η, the same (α, γ) can produce significantly different noise effects on X^{-1} depending on the exponent $\frac{1}{1-\alpha}$.

A very important consequence of our stochastic formulation is that the time of failure becomes a random variable:

$$X : (\Omega, (\mathcal{F}_t)_{t>t_0}, P), \quad t_f(\omega) = \inf\{t : X^{-1}(\omega, t) = 0\},$$

for a.e. $\omega \in \Omega$, where $(\mathcal{F}_t)_{t>t_0}$ is the filtration generated by the noise, and P is a probability measure over it (Karatzas and Shreve, 1991). Plots 2b,d,f display pdf of t_f calculated by Monte Carlo simulation (2,000 samples). The pdf becomes more peaked and symmetric when $\gamma > 0$.

4 The mean-reversion properties

Let $\hat{\eta}$ be the ODE solution with data $\eta(t_0)$ at time t_0. If $\sigma > 0$ and $\gamma = 0$, the law of Brownian Motion and the linearity of the ODE imply that:

$$\eta(t) - \hat{\eta}(t) \sim \mathcal{N}\left(0, \sigma^2(t - t_0)\right).$$

If $\gamma > 0$ then $|\eta(t) - \hat{\eta}(t)|$ is reduced to zero exponentially. If $\sigma = 0$ and the equation starts with $\delta(t_0) := |\eta(t_0) - \hat{\eta}(t_0)| > 0$ we have:

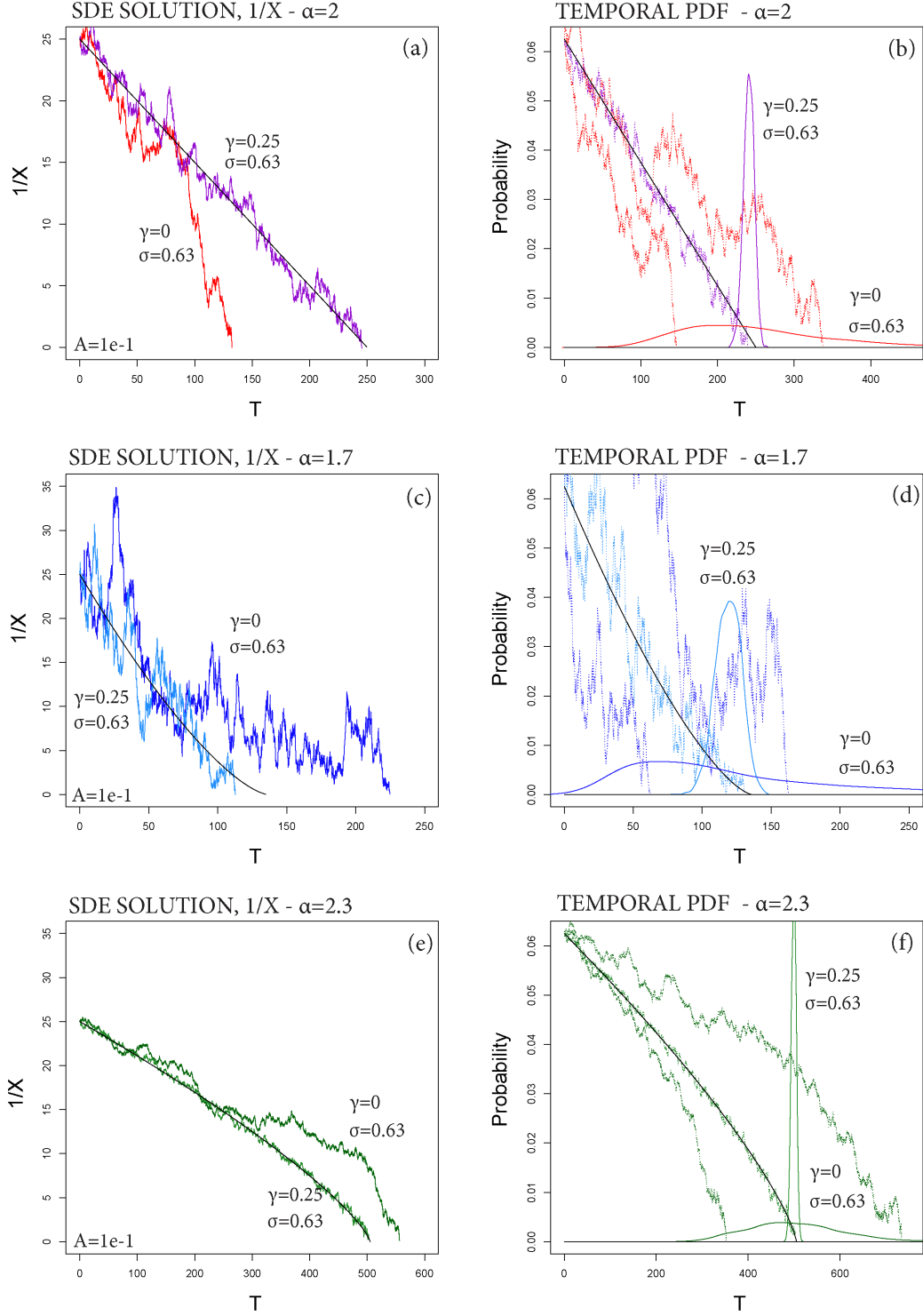$$\delta(t) := |\eta(t) - \hat{\eta}(t)| = \exp[-\gamma(t - t_0)].$$

Figure 2: SDE solutions, $1/X$, (a,b) with $\alpha = 2$, (c,d) with $\alpha = 1.7$, (e,f) with $\alpha = 2.3$. A black line marks the mean solution. In (a,c,e) the colored lines are random paths, with $\gamma = 0$ or $\gamma = 0.25$. In (b,d,f) the colored lines are the pdfs of t_f and the dotted lines are random paths.

Figure 3a shows this example, and $3\gamma^{-1}$ provides the time interval required to have $\delta(t) \simeq \delta(t_0)/20$. If both $\sigma > 0$ and $\gamma > 0$, the combined effect of the *noise* and the *mean-reversion* defines the Ornstein-Uhlenbeck process (from equation 5, with $A = 0$ and $\eta_{t_0} = 0$):

$$d\eta_t = -\gamma\eta_t dt + \sigma dW_t, \tag{7}$$

whose solution is:

$$\eta_t \sim \mathcal{N}\left(0, \frac{\sigma^2}{2\gamma}\left[1 - \exp(-2\gamma t)\right]\right) \simeq \mathcal{N}\left(0, \frac{\sigma^2}{2\gamma}\right), \tag{8}$$

when $\gamma|t_f - t_0| \gg 1$. The constant

$$K := \frac{\sigma^2}{2\gamma}$$

uniquely defines the probability distribution of the solution of this SDE. Different realizations of this process are displayed in in Figure 3b. If σ^2 increases and γ decreases, then the perturbations are more frequent, but reverted faster. This may have some effect on the estimate of t_f, but discrete data cannot provide any information on perturbations occurred at frequency higher than the measurements. In most of our examples we define $\gamma^{-1} = 15$ days. That is, any perturbation decays by 63% within 15 days, and by 95% within 45 days, which is close to the total length of the time interval considered. Sensitivity analysis on this parameter is performed in Appendix A.
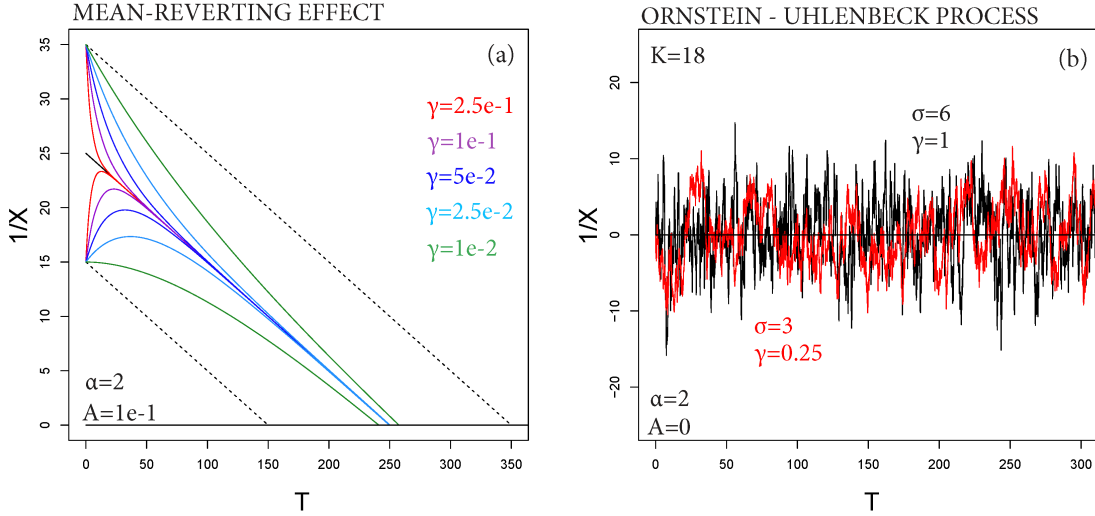

Figure 3: (a) SDE solutions with $\alpha = 2$, 1/X, with $\sigma = 0$, but $\delta(t_0) > 0$. Different colors correspond to different values of γ. (b) Ornstein-Uhlenbeck processes with equal $K = \frac{\sigma^2}{\gamma}$, but different (σ, γ).

5 Parameter fitting and UQ

The application of our method requires the estimation of five parameters:

- *curvature* parameter α,
- *slope* parameter A,
- *noise* parameter σ,
- *mean-reversion* parameter γ,
- an unperturbed initial value $\hat{\eta}(t_0)$.

7

We assume all these parameters to be positive, and $\alpha > 1$. In particular, the case $\alpha = 1$ is trivial, and the cases $\alpha < 1$ or $A \leq 0$ imply $t_f = +\infty$. We note that $\hat{\eta}(t_0)$ cannot be defined equal to the first observation, because of the perturbations.

Several methods have been adopted in the determination of the parameters in the ODE problem (Voight, 1988a; Cornelius and Voight, 1995). The Log-rate versus Log-acceleration Technique (LLT), and the Hindsight Technique (HT) can both provide estimates of α. They are described in Appendix B. The first technique is generally less accurate because it needs an estimate of the time derivative of the observations. The second technique requires that we know t_e and hence can only be used in retrospective analysis. We take advantage of these classical methods to estimate α in our examples, approximating the curvature of the mean solution from the available observations. We remark that the time derivatives are always based on the discrete data in Voight (1988a), and not affected by the roughness of the paths of the new SDE formulation.

If α is given, then a linearized least square method can be used to fit parameter A and $\hat{\eta}(t_0)$ on the inverse plot $1/X$. This is the main method classically adopted as a forecasting technique in the ODE problem. In particular, we apply a linear regressive model to eq. 2:

$$X(t)^{1-\alpha} = (1 - \alpha)A(t - t_0) + \eta(t_0),$$

producing estimates of $(1 - \alpha)A$ and $\hat{\eta}(t_0)$.

Finally, we fit the stochastic parameters σ and γ on the residuals of this linearized problem, imposing the constant $K = \frac{\sigma^2}{2\gamma}$ to be equal to their variance. In summary, we plug-in α from classical LLT or HT, and then we obtain $(A, \hat{\eta}(t_0), K)$ as required to the SDE definition. The numerical solution of the SDE is performed by the Euler-Maruyama method, which is equivalent to the Milstein method in our case.

In the following we apply three different forecast methods on the datasets in Voight (1988a), and we test t_f as an estimator of t_e. In all our methods t_f is assumed as a random variable, and its pdf

$$g_{t_f} : \mathbb{R} \to \mathbb{R}+, \quad \int_0^\infty g_{t_f}(x)dx = 1$$

is estimated following a classical Gaussian kde method.

- Method 1 is based on the classical ODE, and the corresponding forecasts are displayed in Figure 4. This is consistent with the original formulation in Voight (1988a). g_{t_f} depends on the statistical uncertainty affecting the pair $(A, \hat{\eta}(t_0))$ in the regression method. We implement this *model uncertainty* as a bivariate Gaussian in a Monte Carlo of 5,000 samples.

  Methods 2 and 3 are both based on the new SDE.

- In Method 2, the least-square curve is assumed to be the mean solution, and g_{t_f} is defined by the noise. The forecasts are displayed in Figure 5. We implement this *aleatory uncertainty* in a Monte Carlo of 5,000 sample paths of the stochastic noise.

- Method 3 is *doubly stochastic* (e.g. Bevilacqua (2016)). The mean solution is affected first by the statistical uncertainty in the regression method, and then perturbed by the stochastic noise. The values of g_{t_f} are thus reported as 5th percentile, mean, and 95th percentile curves. We remark that the two uncertainties are not independent, because the properties of the noise are related to the residuals in the linearized problem. The forecasts are displayed in Figure 6. In this case, the mean pdf is based on a Monte Carlo sampling consisting of 10,000 model runs, while the percentile values are based on a hierarchical Monte Carlo of $200 \times 300 = 6e4$ samples.

Our four case studies refer to the volcanic eruptions of Mt. St. Helens (USA), 1982 (a) and 1981 (b), and of Bezyamyanny (USSR), 1960 (c), and to the landslide of Mt. Toc (Italy), 1963 (d), which caused the Vajont Dam disaster. These datasets are characterized by different values of α, and by different confidence intervals in the linear regression. Estimates of α are based on data reported in Appendix B.

In general, the mean path is consistent in the three methods, but UQ is significantly different, as well as the values of g_{t_f}. In particular:

(a) Mt. St. Helens, 1982 - line length data values are initially scattered, until $t = t_e - 20$, and then become more aligned. $\alpha \approx 2$, and $E[t_f]$ overestimates t_e of 1-3 days in all the methods. Uncertainty range is twice larger in Method 2 and 3 compared to Method 1.
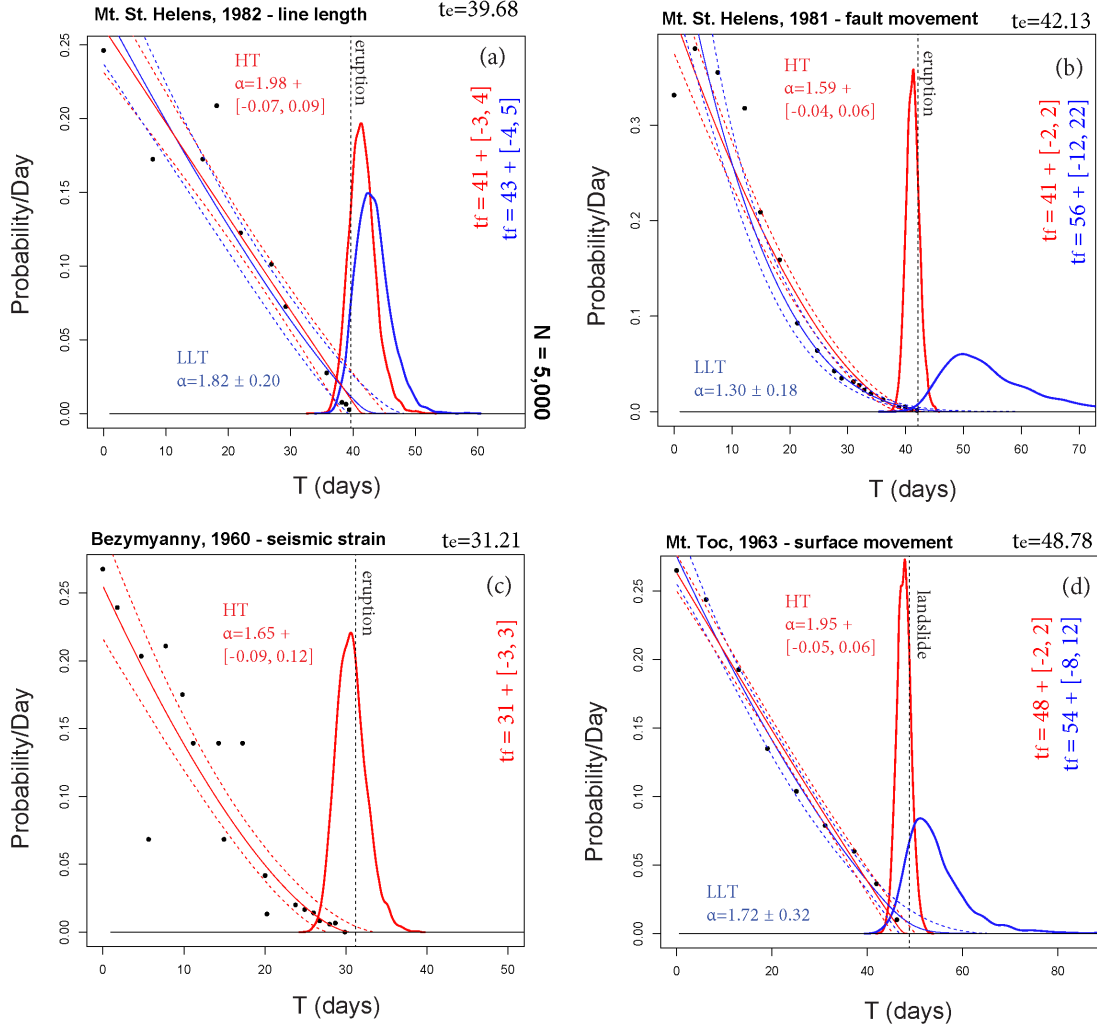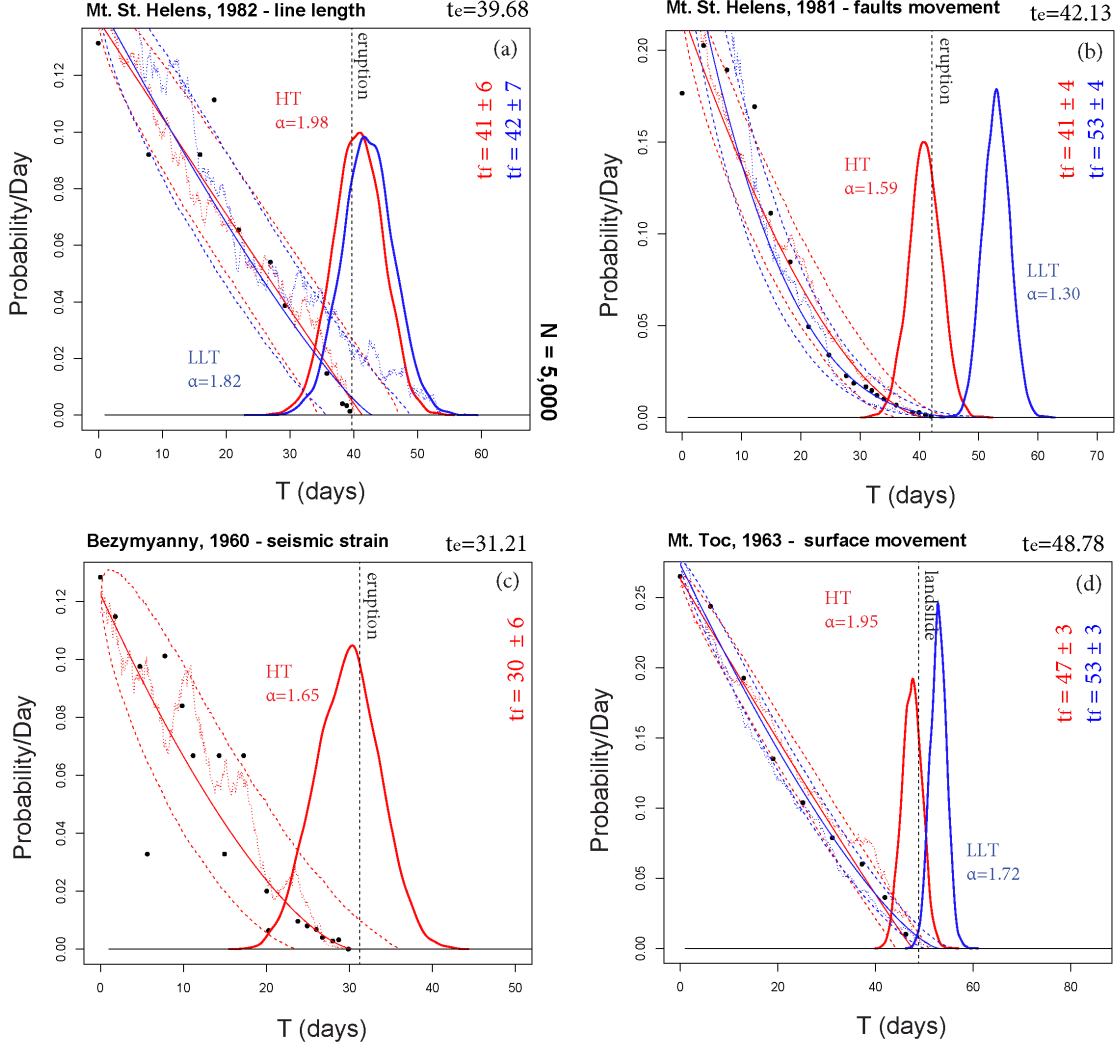
8

Figure 4: Estimators of t_f based on Method 1. Blue lines assume α as from LLT, red as from HT. The bold line is g_{t_f}. Thin dashed lines bound the 90% confidence interval of the ODE paths, and a thin continuous line is the mean path. A dashed black line marks t_e. Method 1 generally provides a good estimator of t_e, but often only the HT method allows these robust estimates.

(b) **Mt. St. Helens, 1981 - fault movement** this example is characterized by $\alpha \approx 1.6$ in HT and $\alpha = 1.3 \pm 0.2$ in LLT. In the first case (red), in all methods $E[t_f]$ underestimates t_e of only 1 day, with uncertainty range ± 2 days in Method 1, and twice larger in Method 2 and 3. The second case (blue) is less accurate. In Method 1, 2 and, 3 $E[t_f]$ overestimates t_e of 14, 11, and 14 days, respectively. Always outside the uncertainty range. However, in Method 3 the 95th percentile plot is above 9% at time t_e.

(c) **Bezymyanny, 1960 - seismic strain** data values are persistently scattered until $t = t_e - 10$, and $\alpha \approx 1.6$. In Method 1, $E[t_f]$ correctly estimates t_e, with uncertainty range of ± 3 days. In Methods 2 and 3, $E[t_f]$ underestimates t_e of 1 day with an uncertainty range twice large.

(d) **Mt. Toc, 1963 - surface movement** According to HT, $\alpha \approx 2$, while according to LLT, $\alpha = 1.7 \pm 0.3$. In the first case (red), in Method 1 and 3 $E[t_f]$ correctly estimates t_e, in Method 2 it underestimates in of 1 day. Uncertainty range is ± 2 days in Method 1, ± 3 in Method 2, ± 4

9

in Method 3. In the second case (blue), in Method 1 $E[t_f]$ overestimates t_e of 5 days, but the uncertainty range is about ±10 days and captures it. In Method 2 $E[t_f]$ overestimates t_e of 4 days, but uncertainty is reduced to ±3 days. Method 3 gives very similar results to Method 1, and the 95th percentile plot is above 20% at time t_e.

Figure 5: Estimators of t_f based on Method 2. Blue lines assume α as from LLT, red as from HT. A bold line is g_{t_f}. Thin dashed lines bound the 90% confidence interval of the SDE paths, and a thin continuous line is the mean path. Thin dotted lines show examples of random paths. A dashed black line marks t_e. Method 2 reduces the overestimation issues of Method 1, but model uncertainty is neglected.

In summary, when $\alpha \approx 2$ Method 1 generally provides a good estimator of t_e, as well as Methods 2 and 3. They generally have larger uncertainty ranges. Sometimes, when $\alpha \leq 1.6$, Method 1 tends to overestimate t_e. Method 2 reduces this issue, but model uncertainty is neglected and the estimate still misses t_e. Method 3 enhances Method 2, and its doubly stochastic nature allows the production of either mean probability values or more conservative 95th percentile values, with significantly high probability of eruption at time t_e, even when the mean estimate fails the forecast.
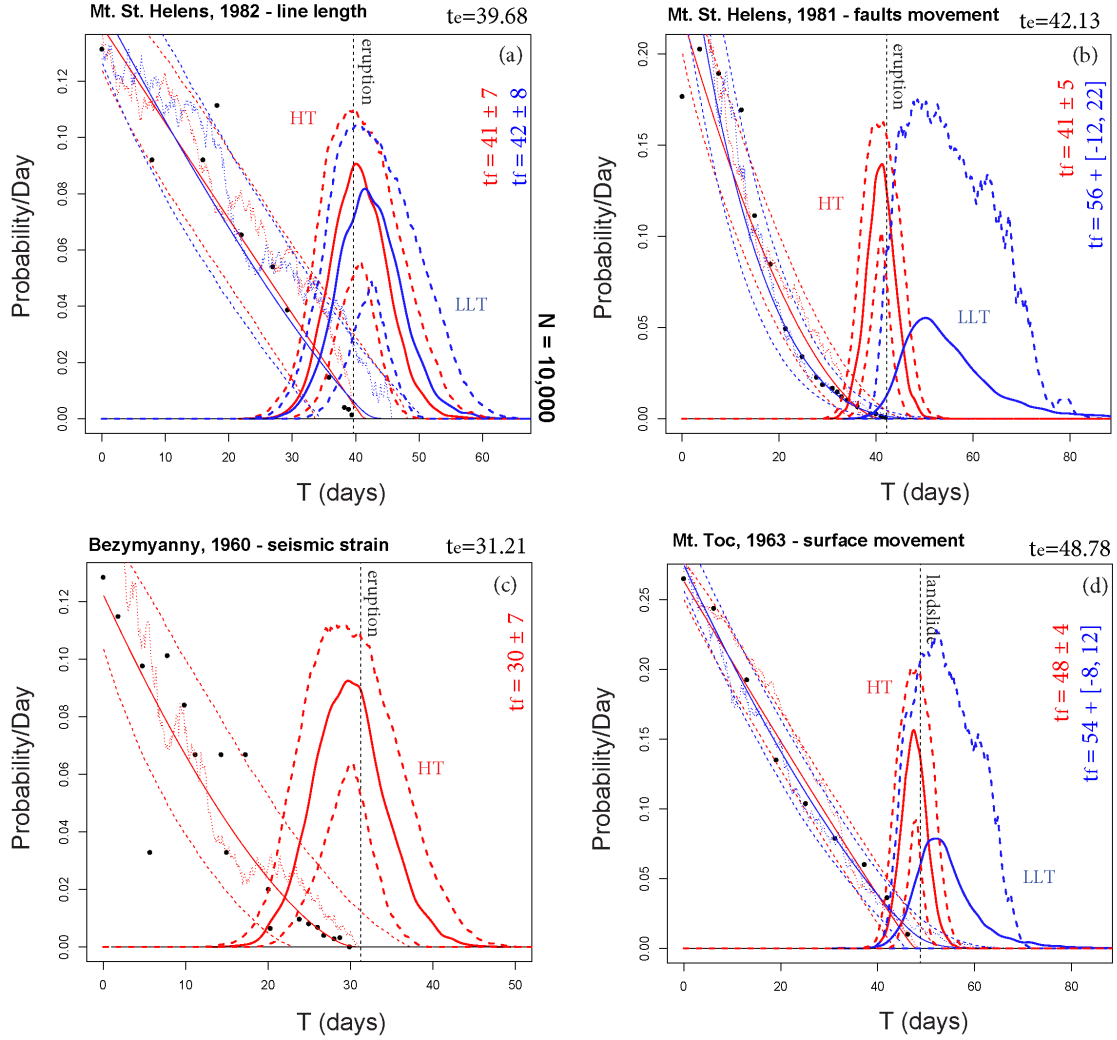
Figure 6: Estimators of t_f based on Method 3. Blue lines assume α as from LLT, red as from HT. A bold line is g_{t_f}, and bold dashed lines are its 5th and 95th percentile values. Thin dashed lines bound the 90% confidence interval of the SDE paths, and a thin continuous line is the mean path. Thin dotted lines show examples of random paths. A dashed black line marks t_e. Method 3 enhances Method 2 and performs significantly better.

6 Examples of probability forecasts

The estimators defined in the previous section are informed by the entire sequence of data, up to the eruption onset or landslide initiation t_e. This provides useful insight on the validity of the model, but it is not a forecast (Boué et al., 2015). Indeed in any forecasting problem the sequence of data is available up to a time $t_1 < t_e$, that represents the current time of the forecast. All the data collected after time t_1 cannot be considered.

In the following figures we display forecasts of t_e based on the ODE method, and obtained from the data collected in a limited time window $T = [t_2, t_1]$. We focus on the two examples of Mt. St. Helens, 1982 - line length ($\alpha \approx 1.98$), and Bezymyanny, 1960 - seismic strain ($\alpha \approx 1.65$).
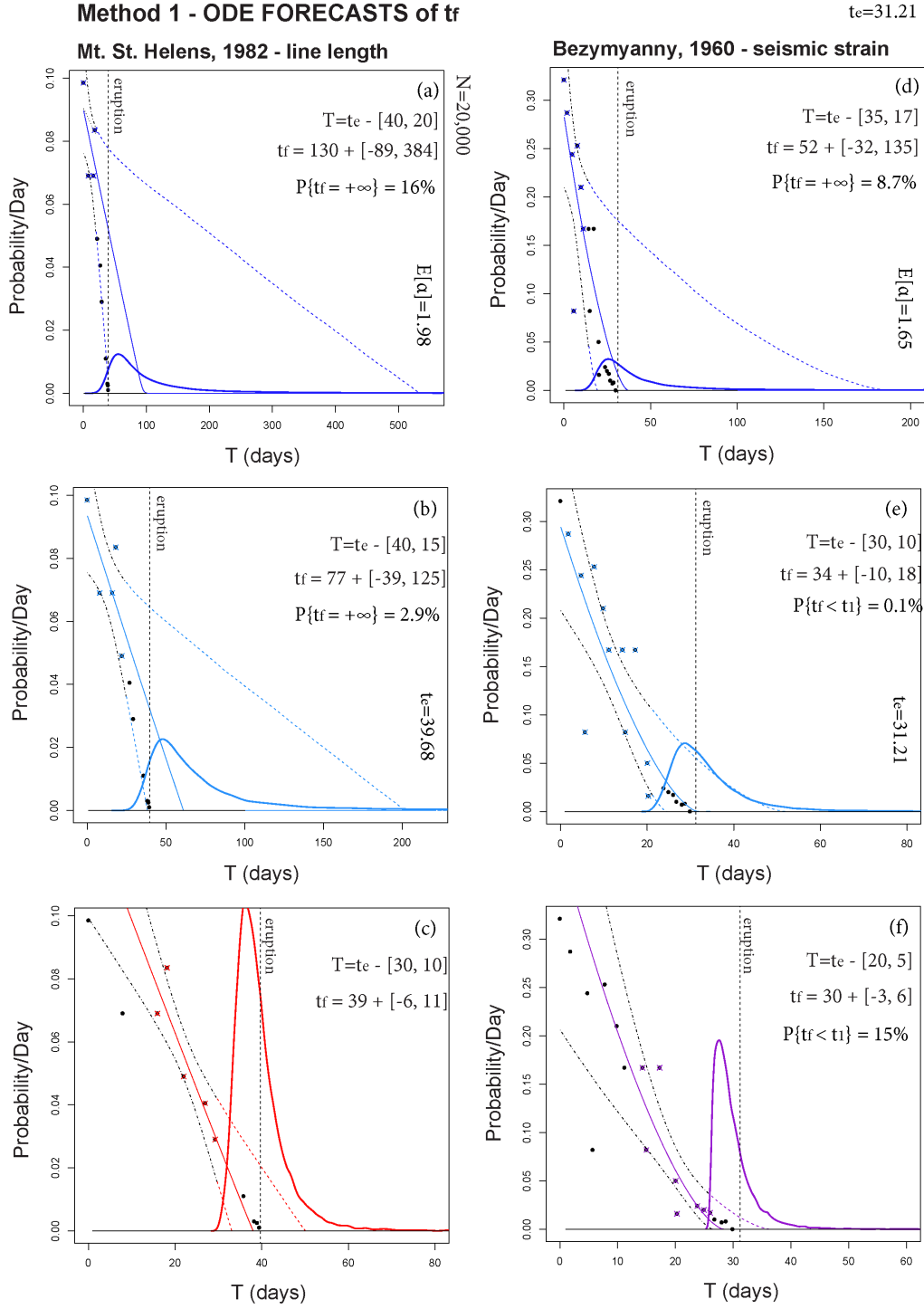
Figure 7: Forecasts of t_f based on Method 1. In (a,b,c) and (d,e,f) two examples are tested on three different time windows T. The bold line is g_{t_f}. Thin dashed lines bound the 90% confidence interval of the ODE paths, and a thin continuous line is the mean path. A dashed black line marks t_e.
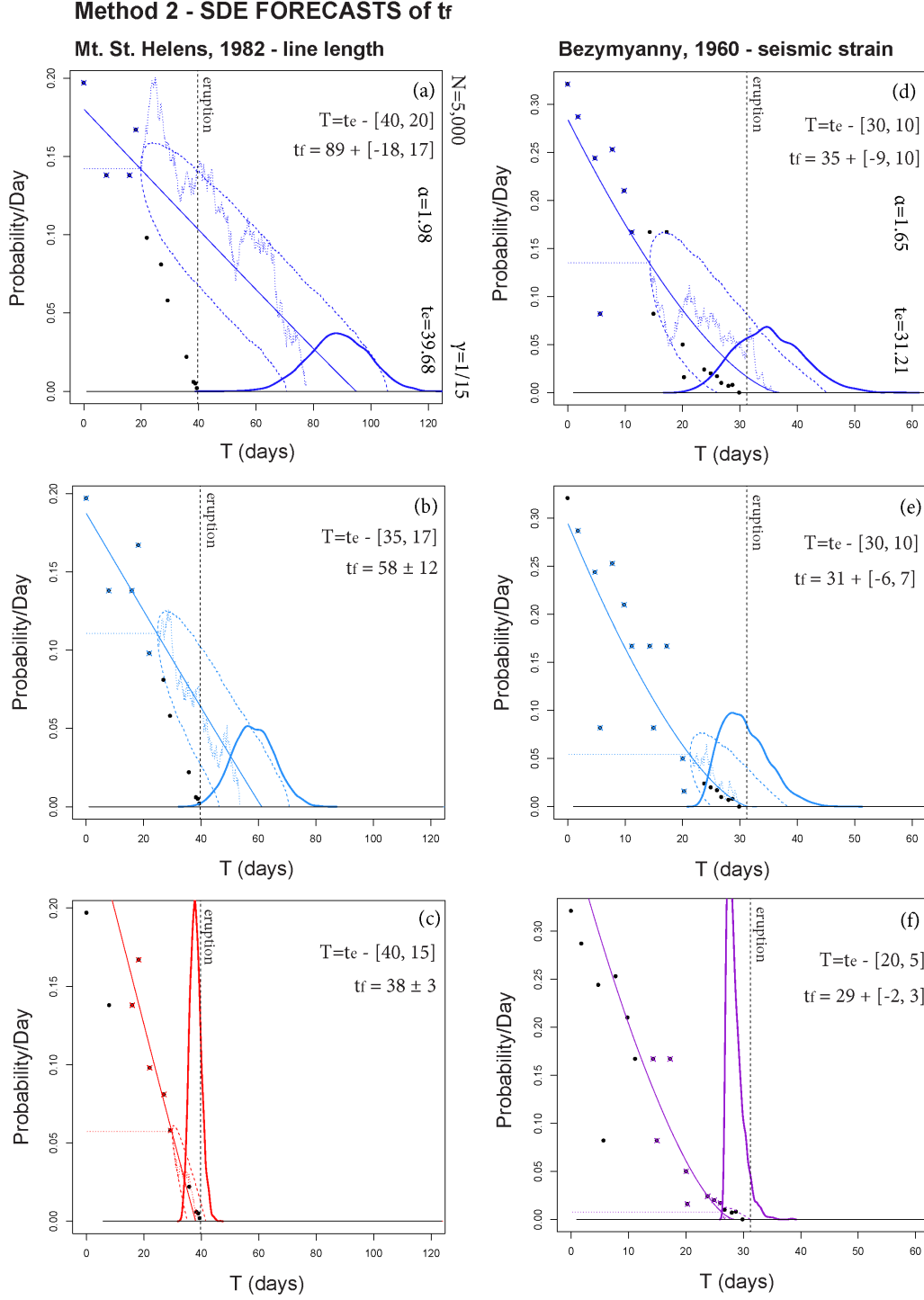
Figure 8: Forecasts of t_f based on Method 2. In (a,b,c) and (d,e,f) two examples are tested on three different time windows T. The bold line is g_{t_f}. Thin dashed lines bound the 90% confidence interval of the SDE paths, and a thin continuous line is the mean path. Thin dotted lines show examples of random paths. A thin dashed line marks $1/x_0$, and a dashed black line marks t_e.
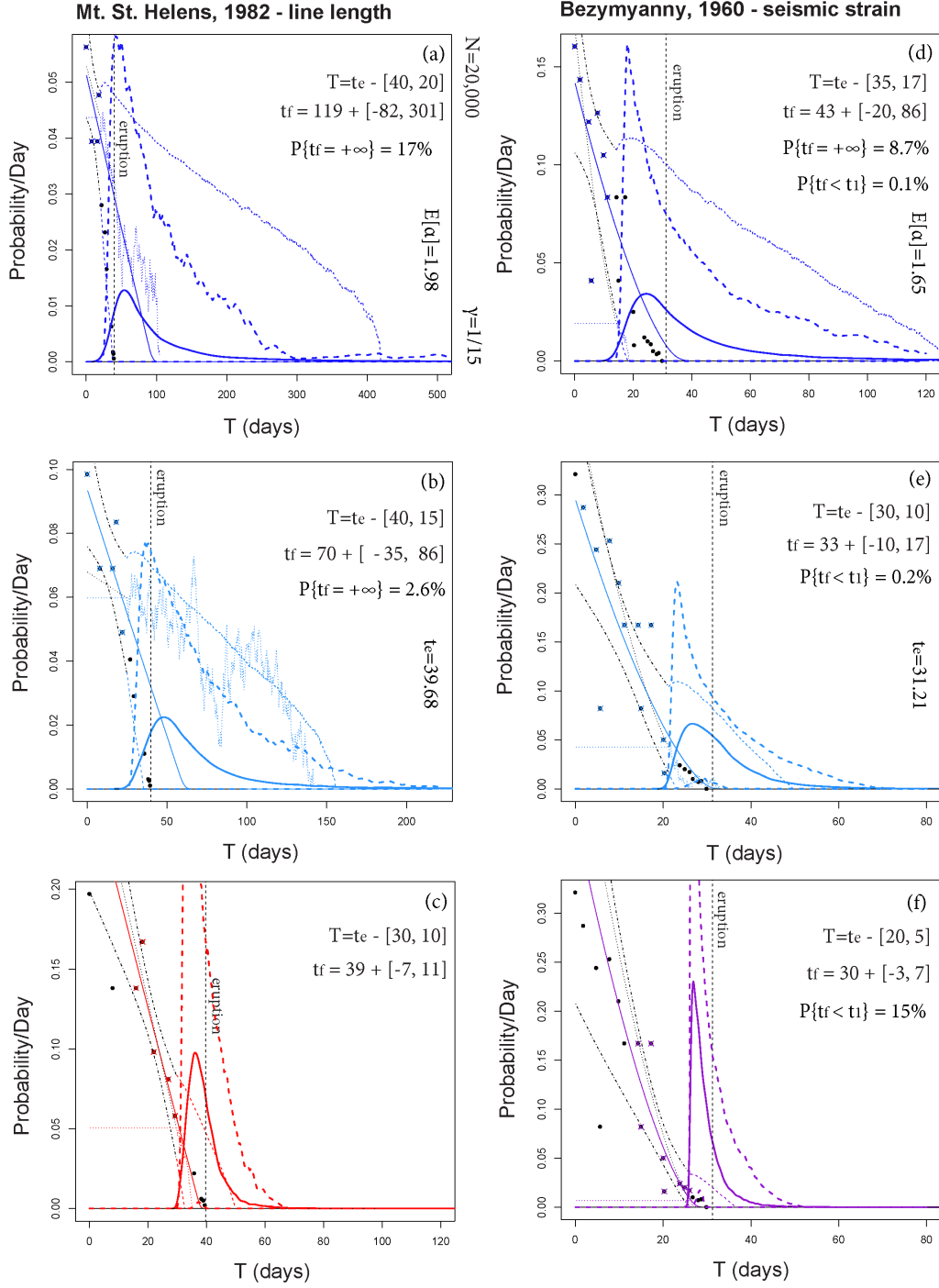
13

Figure 9: Forecasts of t_f based on Method 3. In (a,b,c) and (d,e,f) two examples are tested on three different time windows T. The bold line is g_{t_f}, and bold dashed lines are its 5th and 95th percentile values. Thin dashed lines bound the 90% confidence interval of the SDE paths, and a thin continuous line is the mean path. Thin dotted lines show examples of random paths. A thin dashed line marks $1/x_0$, and a dashed black line marks t_e.

14

Figure 7 adopts Method 1, Figure 8 Method 2 and Figure 9 Method 3. Method 1 and mean pdf in Method 3 both implement a Monte Carlo of 20,000 samples, Method 2 a Monte Carlo of 5,000 samples, the percentile values in Method 3 are based on a hierarchical Monte Carlo of $300 \times 500 = 1.5e5$ samples.

Forecasting results can be significantly uncertain, because they are inherently extrapolations based on past data. In Methods 1 and 3, sometimes $P\{t_f = \infty\} > 0$ and there is a non-negligible chance that the solution path never hits the real axis. In contrast, if $P\{t_f < t_1\} > 0$ there is a chance that $\hat{\eta}(t_1) < 0$ and the equation is not well defined. The probability of both these events is quantified.

In our examples we consider three time windows progressively moving towards t_e, including new observations and neglecting the old data. In particular, (a,d) rely on the initial scattered data, (b,e) include both scattered and aligned observations, (c,f) generally forget about scattered data. We remark that α remains fixed for simplicity.

In general, uncertainty is always reduced while getting closer to t_e. In particular:

Mt. St. Helens, 1982 - line length (a) If $t_1 = t_e - 20$, in Method 1 $E[t_f]$ overestimates t_e of 90 days, in Method 2 of 40, in Method 3 of 80. Uncertainty is $[-89, +384]$ in Method 1, $[-18, +17]$ in Method 2, and $[-82, +301]$ in Method 3. Only in Method 2 $E[t_f]$ falls outside the uncertainty range, and 95th percentile plot in Method 3 is about 6% at time t_e. In Methods 1 and 3, $P\{t_f = \infty\} > 15\%$.

(b) If $t_1 = t_e - 15$, in Method 1 $E[t_f]$ overestimates t_e of 37 days, in Method 2 of 18, in Method 3 of 30. Uncertainty is $[-39, +125]$ in Method 1, ± 12 in Method 2, and $[-35, +86]$ in Method 3. Again only in Method 2 $E[t_f]$ falls outside the uncertainty range, and 95th percentile plot in Method 3 is about 8% at time t_e. In Methods 1 and 3, $P\{t_f = \infty\} \approx 2\%$.

(c) If $t_1 = t_e - 10$, in Method 1 $E[t_f]$ estimates correctly t_e, with an uncertainty range of $[-6, +11]$ days. In Method 2 $E[t_f]$ underestimates t_e of 1, with an uncertainty range of ± 3. Method 3 performs similarly to Method 1, and its 95th percentile plot is about 16% at time t_e.

Bezymyanny, 1960 - seismic strain (d) If $t_1 = t_e - 17$, in Method 1 $E[t_f]$ overestimates t_e of 21 days, in Method 2 of 4, in Method 3 of 12. Uncertainty is $[-32, +135]$ in Method 1, $[-9, +10]$ in Method 2, and $[-20, +86]$ in Method 3. In all methods $E[t_f]$ falls inside the uncertainty range, and 95th percentile plot in Method 3 is about 7.5% at time t_e. In Methods 1 and 3, $P\{t_f = \infty\} \approx 9\%$.

(e) If $t_1 = t_e - 10$, in Method 1 $E[t_f]$ overestimates t_e of 3 days, in Method 2 estimates t_e correctly, in Method 3 overestimates t_e of 2 days. Uncertainty is $[-10, +18]$ in Method 1, $[-6, +7]$ in Method 2, and $[-10, +17]$ in Method 3. The 95th percentile plot in Method 3 is about 10% at time t_e.

(f) If $t_1 = t_e - 5$, in Method 1 $E[t_f]$ underestimates t_e of 1 day, in Method 2 of 2. Method 3 performs similarly to Method 1. Uncertainty is $[-3, +6]$ in Method 1, $[-2, +3]$ in Method 2, and $[-3, +7]$ in Method 3. The 95th percentile plot in Method 3 is about 16% at time t_e. We remark that in Methods 1 and 3, $P\{t_f < t_1\} \approx 15\%$.

In summary, forecasting results of Method 1 and Method 3 are similar, but the more complex UQ related to Method 3 improves its performance. In particular, when the forecast is not well constrained, Method 3 generally reduces the uncertainty range of the estimates if compared to Method 1. Method 2 tends to give a correct forecast only when the eruption is close. The doubly stochastic formulation of Method 3 appears to be impactful, and the 95th percentile of the eruption probability is significant at time t_e.

7 Discussion

We described three different methods for estimating t_f, the ODE-based Method 1, the new SDE-based Method 2, and its doubly stochastic formulation Method 3. We tested the methods in four case studies, and in two of them we also performed forecasts on moving time windows.

Figure 10 summarizes the likelihood $g_{t_f}(t_e)$, reported as a probability percentage. Plot (a) compares Method 1 (black bars) and Method 2 (colored bars). Method 1 always outperforms Method 2 when α is based on the more accurate HT (red bars), and provides likelihoods above 15%. In contrast, when α is based on LLT (blue bars) the two methods provide lower likelihoods, below 1% in some case. Plot (b) displays the likelihood provided by the doubly stochastic Method 3. Full colored bars report the mean likelihood, shaded bars the 95th percentiles of the likelihood. Mean likelihoods are very similar or above

those provided by Method 2. The 95th percentile values are significantly higher. In particular, when α is based on LLT (blue bars), Method 3 percentiles are all higher than in Method 1.
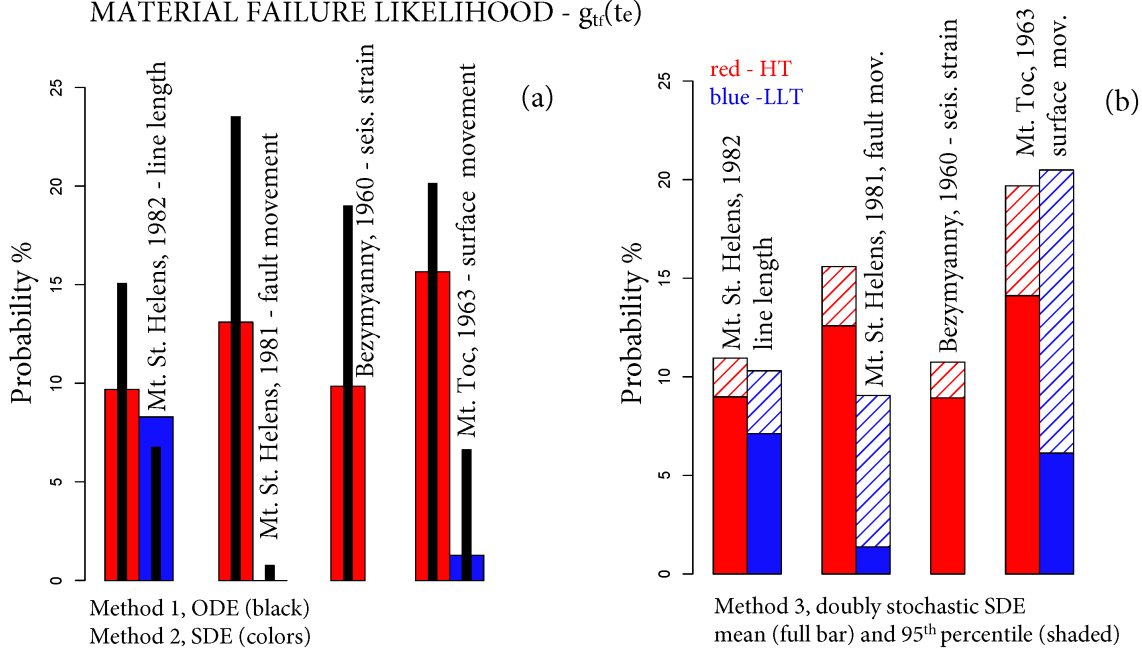

Figure 10: Barplots of the likelihood $g_{t_f}(t_e)$. In plot (a) the black bars assume Method 1, the colored bars Method 2. Plot (b) assumes Method 3, and the full bars are the mean values, and the shaded bars are the 95th percentile values of the likelihood.

These features are confirmed and strengthened in the forecasting examples based on the moving windows. Figure 11 summarizes the corresponding $g_{t_f}(t_e)$. Plot (a) compares Method 1 (black bars) and Method 2 (colored bars). In Mt. St. Helens, 1982 - line length (blue), Method 2 outperforms Method 1 only in the third time window, with the only likelihood above 10%. In Bezymyanny, 1960 - seismic strain (red), Method 2 outperforms Method 1 in the first two time windows, with likelihoods above 5%. Plot (b) concerns the doubly stochastic Method 3. Full colored bars report the mean likelihood, shaded bars its 95th percentile values. In this case, mean likelihoods are very similar to those provided by Method 1. The 95th percentile values are again significantly higher, from 5% to 10% in the first and second time windows, and above 15% in the third.

8 Conclusions

In this study, we have introduced a new doubly stochastic method for performing material failure forecasts. The method enhances the well known FFM equation, introducing a new formulation similar to the Hull-White model. The model is a mean-reverting SDE, which assumes the traditional ODE as the mean solution. New parameters include the noise standard deviation σ and the mean-reversion rapidity γ. They are estimated based on the properties of the residuals in the original linearized problem. The implementation allows the model to make excursions from the classical solutions, including the possibility of some degree of aleatory uncertainty in the estimation. This provides probability forecasts instead that deterministic predictions.

We compared the new method and the forecasting method based on the classical formulation. We also compared an Hull-White model without considering the model uncertainty, and its doubly stochastic formulation. A comparison is performed on four historical datasets of precursory signals already studied

with the classical FFM, including line-length and fault movement at Mt. St. Helens, 1981-82, seismic signals registered from Bezymyanny, 1960, and surface movement of Mt. Toc, 1963. We also considered forecasting problems over moving time windows, based on data in the case studies of Mt. St. Helens, 1982 and Bezymyanny, 1960. The data shows the performance of the methods across a range of possible values of convexity α and amounts of scattering in the observations, and the increased forecasting skill of the doubly stochastic formulation in Method 3.
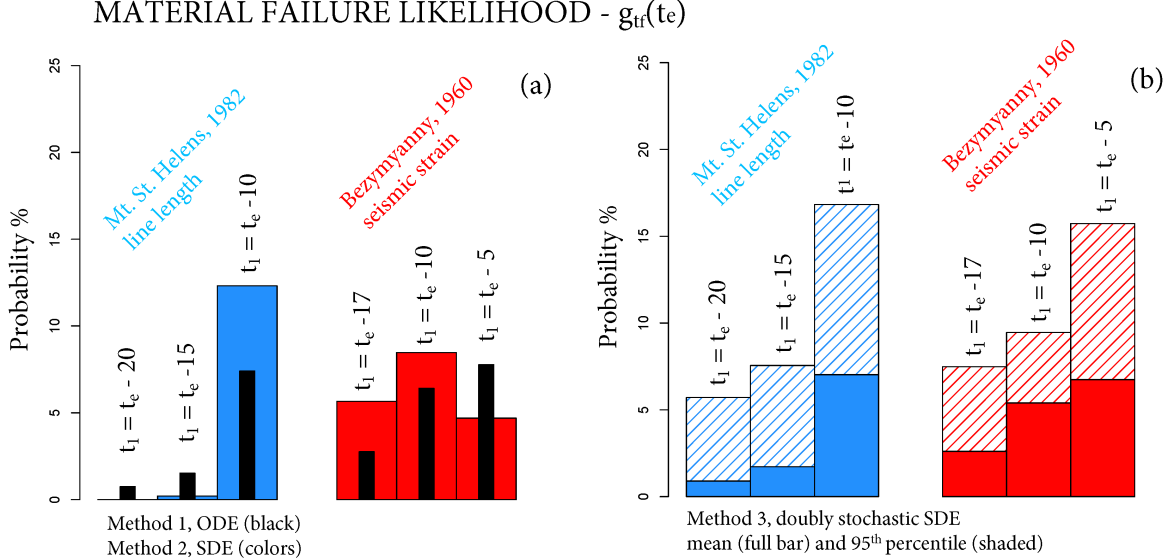

Figure 11: Barplots of the likelihood $g_{t_f}(t_e)$ in two forecasting examples, on three different time windows. In plot (a) the black bars assume Method 1, the colored bars Method 2. Plot (b) assumes Method 3, and the full bars are the mean values, and the shaded bars are the 95th percentile values of the likelihood.

The doubly stochastic formulation is particularly impacting in the forecasts because it enables the calculation of the 95th percentiles of the probability of failure. This values are generally higher than the mean estimates, and represent the *worst case scenario* with a probability of occurrence above 5%. This was not possible in the classical formulation. This approach is the subject of ongoing and future work, with the purpose to further enhance the short-term eruption forecasting robustness.

Acknowledgements

A   Sensitivity analysis on the noise properties

Discrete observations provide us information on $K = \frac{\sigma^2}{\gamma}$, which is the variance of the solution of the Ornstein-Uhlenbeck process associated to our SDE. However, solutions with the same K can look significantly different, as shown in Figure 3b.

The estimators in all our case studies assume $\gamma = 1/15$. This is a choice based on the empirical observation that the total length of temporal sequence is at the scale of 45 days, and the duration of well-aligned observations is at the scale of 15 days. In Figure 12 we show examples of solutions with doubled or halved γ. There is an apparent effect on the 90% confidence interval of the SDE paths, which is enlarged increasing γ, and terminally bent down towards the real axis. This is increased in (c,d), where

$\alpha = 1.65$. However, even in that case the effect of g_{t_f} is minor, and increasing γ of four times reduces $E[t_f]$ of about 5 days.
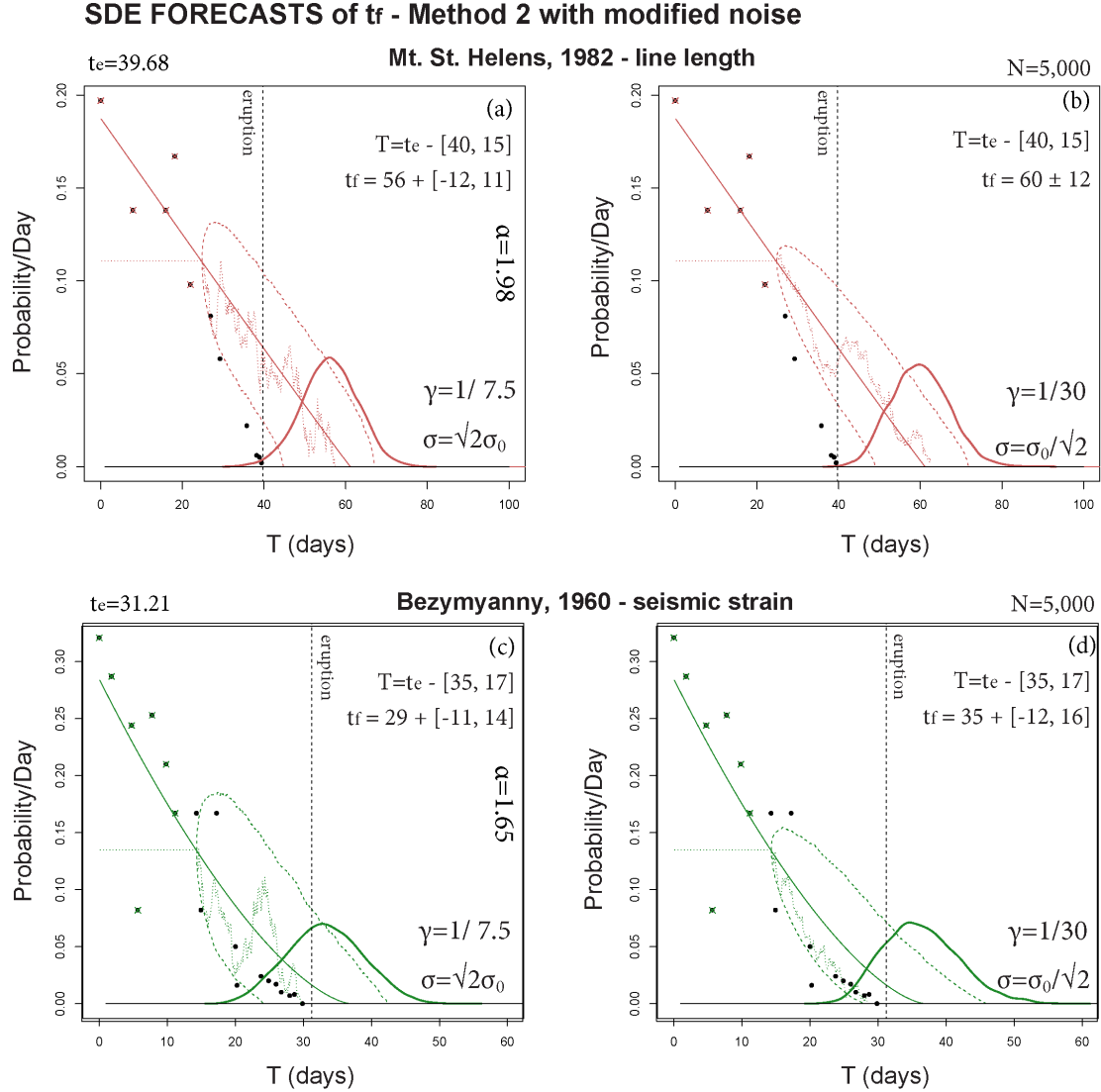

Figure 12: Forecasts of t_f based on Method 2. The solutions assume equal $K = \frac{\sigma^2}{\gamma}$, but different (σ, γ). In plots (a,c) $\gamma^{-1} = 7.5$, and in plots (b,d) $\gamma^{-1} = 30$. The bold line is the pdf of t_f. Thin dashed lines bound the 90% confidence interval of the SDE paths, and a thin continuous line is the mean path. The thin dotted lines are random paths. A thin dashed line marks $1/x_0$, and a dashed black line marks t_e.

B   Classical statistical analysis of FFM

In our study we apply a linearized least-squared approach, based on a preliminary estimate of α. Nonlinear regression methods have also been applied to the ODE problem, but in this study we relied on the linearized method for simplicity (Bell et al., 2011). Linear regressive models based on different formulations of the differential equation can provide estimates of α. Even if these formulations are algebraically

18

equivalent, the result of the regression can change significantly. The two different methods LLT and HT are reported in Voight (1988a) and then further detailed in Cornelius and Voight (1995).
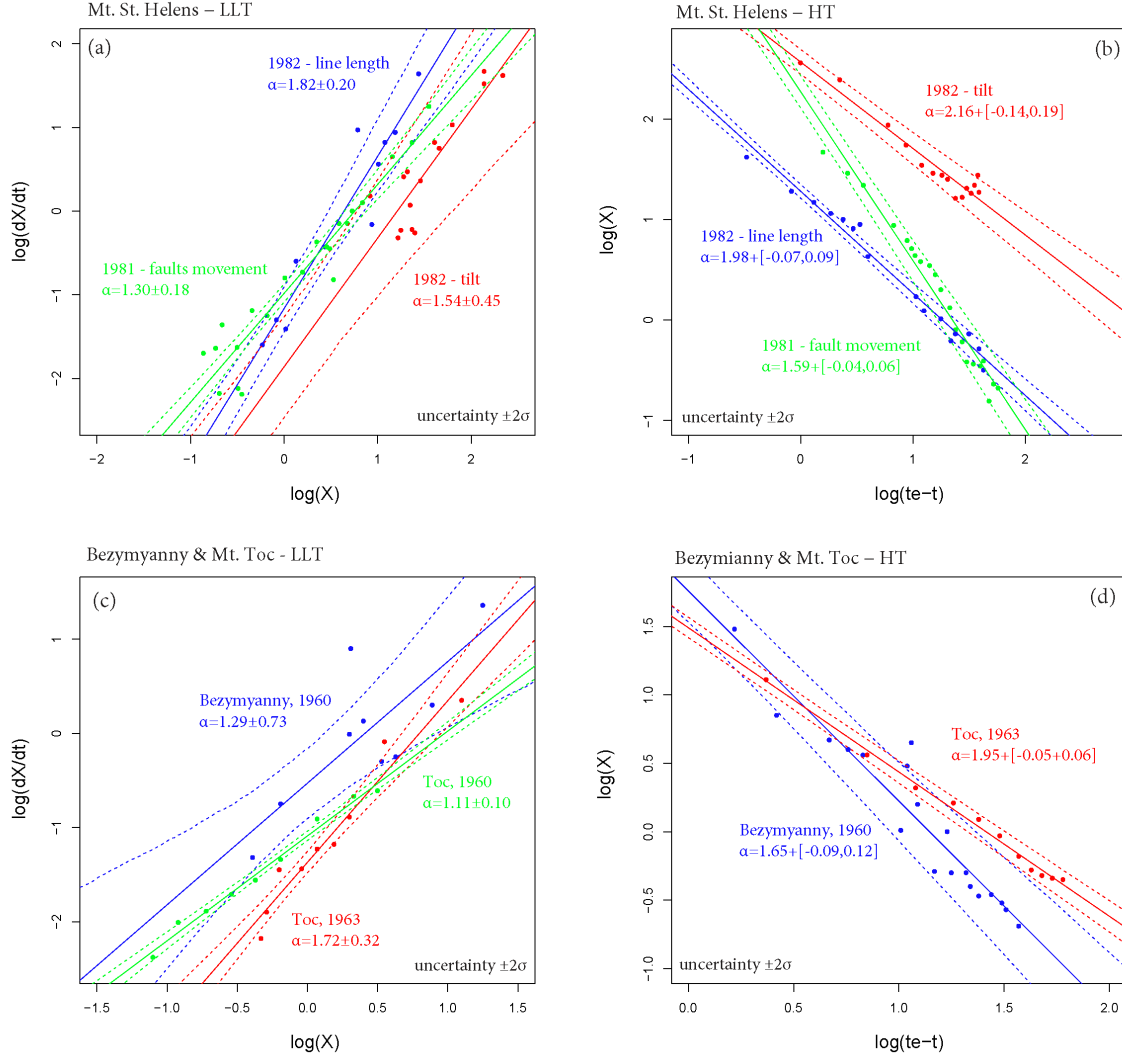

Figure 13: Methods LLT and HT applied to (a,b) St. Helens and (c,d) Bezymyanny&Mt. Toc datasets. Different colors correspond to different data. Dashed lines bound the 90% confidence interval of the regression line. Figure modified from Voight (1988a).

The Log-rate versus log-acceleration technique (LLT), is the application of a linear regressive model (LRM) on the equation (from eq. 1):

$$\log\left(\frac{dX}{dt}\right) = \alpha \log(X) + \log(A)$$

can produce estimates of α and $\log(A)$. It requires an approximation to the rate change, which typically suffers of data scattering. Then, A is not robustly constrained by its logarithm. Moreover, the equation may be not well-posed in case of negative rates, requiring to neglect some values, or to apply the equation to $X + c > 0$.

In the Hindsight technique (HT), a LRM is applied to the equation (from eq. 3, with $t_0 = t_f$):

$$\log(X(t)) = \frac{1}{1-\alpha} \log(t_f - t) + \frac{\log[A(\alpha-1)]}{1-\alpha},$$

19

producing estimates of $\frac{1}{1-\alpha}$ and $\frac{\log[A(\alpha-1)]}{1-\alpha}$. It does not rely on the rate change, but requires to know the failure time t_f in advance. This is the reason of its name. Thus, it is not a method producing forecasts, but can be solely used in retrospective analysis. Moreover, while the value of α is well constrained, the value of A is not. The uncertainty range affecting A is increased by the uncertainty affecting α, and the estimate is done in logarithmic scale.

Figure 13 shows the results of the LLT and HT applied to the Mt. St. Helens (a,b), and to the Bezyamyanny & Mt. Toc datasets (c,d). We note that the accuracy of HT is generally higher. In our examples we implemented seven datasets already processed in Voight (1988a), discarding four of them. These would require a more detailed UQ of the unprocessed data source. In detail, the Mt. St. Helens tilt dataset shows significantly discordant results between LLT and HT, and both the datasets are excluded. The uncertainty affecting α in the Bezymyanny dataset according to LLT is very large and is partially supported below 1. The LLT results of the Mt. Toc, 1960 dataset are characterized by $\alpha \approx 1$ and a very low scattering, insufficient to define a significant noise.

References

Bebbington, M. S. (2013). Assessing spatio-temporal eruption forecasts in a monogenetic volcanic field. *Journal of Volcanology and Geothermal Research*, 252(Supplement C):14 – 28.

Bell, A. F., Naylor, M., Heap, M. J., and Main, I. G. (2011). Forecasting volcanic eruptions and other material failure phenomena: An evaluation of the failure forecast method. *Geophysical Research Letters*, 38(15):5.

Bell, A. F., Naylor, M., and Main, I. G. (2013). The limits of predictability of volcanic eruptions from accelerating rates of earthquakes. *Geophysical Journal International*, 194(3):1541–1553.

Bevilacqua, A. (2016). *Doubly stochastic models for volcanic hazard assessment at Campi Flegrei caldera*, volume 21 of *Theses*. Edizioni della Normale, Birkhäuser/Springer.

Bevilacqua, A., Bursik, M., Patra, A., Pitman, E., Qingyuan, Y., Sangani, R., and Kobs-Nawotniak, S. (2018). Late Quaternary eruption record and probability of future volcanic eruptions in the Long Valley volcanic region (CA, USA). *Journal of Geophysical Research: Solid Earth*, in press. doi:10.1029/2018JB015644.

Bevilacqua, A., Bursik, M., Patra, A., Pitman, E., and Till, R. (2017a). Bayesian construction of a long-term vent opening map in the Long Valley volcanic region, (CA, USA). *Statistics in Volcanology*, 3(1):1–36.

Bevilacqua, A., Flandoli, F., Neri, A., Isaia, R., and Vitale, S. (2016). Temporal models for the episodic volcanism of Campi Flegrei caldera (Italy) with uncertainty quantification. *Journal of Geophysical Research: Solid Earth*, 121(11):7821–7845.

Bevilacqua, A., Isaia, R., Neri, A., Vitale, S., Aspinall, W. P., Bisson, M., Flandoli, F., Baxter, P. J., Bertagnini, A., Esposti Ongaro, T., Iannuzzi, E., Pistolesi, M., and Rosi, M. (2015). Quantifying volcanic hazard at Campi Flegrei caldera (Italy) with uncertainty assessment: 1. Vent opening maps. *Journal of Geophysical Research: Solid Earth*, 120(4):2309–2329.

Bevilacqua, A., Neri, A., Bisson, M., Esposti Ongaro, T., Flandoli, F., Isaia, R., Rosi, M., and Vitale, S. (2017b). The effects of vent location, event scale, and time forecasts on pyroclastic density current hazard maps at Campi Flegrei caldera (Italy). *Frontiers in Earth Science*, 5:72.

Boué, A., Lesage, P., Cortés, G., Valette, B., and Reyes Dávila, G. (2015). Real-time eruption forecasting using the material Failure Forecast Method with a Bayesian approach. *Journal of Geophysical Research: Solid Earth*, 120(4):2143–2161.

Budi-Santoso, A., Lesage, P., Dwiyono, S., Sumarti, S., Subandriyo, Surono, Jousset, P., and Metaxian, J.-P. (2013). Analysis of the seismic activity associated with the 2010 eruption of Merapi Volcano, Java. *Journal of Volcanology and Geothermal Research*, 261:153 – 170. Merapi eruption.

Chardot, L., Jolly, A. D., Sherburn, S., Fournier, N., and Kennedy, B. (2013). The material failure forecast method as a potential eruption forecasting tool: application to the 2012 unrest episode at White Island volcano, New Zealand. In *IAVCEI 2013 Scientific Assembly, Kagoshima, Japan*.

Chiodini, G., Paonita, A., Aiuppa, A., Costa, A., Caliro, S., De Martino, P., Acocella, V., and Vandemeulebrouck, J. (2016). Magmas near the critical degassing pressure drive volcanic unrest towards a critical state. *Nature Communications*, 7:1–9.

Cornelius, R. and Voight, B. (1994). Seismological aspects of the 1989-1990 eruption at Redoubt Volcano, Alaska: the Materials Failure Forecast Method (FFM) with RSAM and SSAM seismic data. *Journal of Volcanology and Geothermal Research*, 62:469–498.

Cornelius, R. and Voight, B. (1995). Graphical and PC-software analysis of volcano eruption precursors according to the Material Failure Forecast Method (FFM). *Journal of Volcanology and Geothermal Research*, 64:295–320.

Cornelius, R. and Voight, B. (1996). Real time seismic amplitude measurement (RSAM) and seismic spectral amplitude measurement (SSAM) analyses with the material failure forecast method (FFM), June 1991 explosive eruption at Mount Pinatubo. In *Geophysical Unrest*.

Fukuzuno, T. (1985). A method to predict the time of slope failure caused by rainfall using the inverse number of velocity of surface displacement. *Journal of Japanese Landslide Society*, 22:8 – 14.

Hull, J. and White, A. (1990). Pricing Interest Rate Derivatives Securities. *The Review of Financial Studies*, 3:573592.

Karatzas, I. and Shreve, S. E. (1991). *Brownian Motion and Stochastic Calculus*. Springer; Berlin, Heidelberg, New York.

Kilburn, C. R. (2003). Multiscale fracturing as a key to forecasting volcanic eruptions. *Journal of Volcanology and Geothermal Research*, 125(3):271 – 289.

Kilburn, C. R. J. and Voight, B. (1998). Slow rock fracture as eruption precursor at Soufriere Hills Volcano, Montserrat. *Geophysical Research Letters*, 25(19):3665–3668.

Lavallée, Y., Meredith, P. G., Dingwell, D., Hess, K., Wassermann, J., Cordonnier, B., Gerik, A., and Kruhl, J. H. (2008). Seismogenic lavas and explosive eruption forecasting. *Nature*, 453:507 – 510.

Marzocchi, W. and Bebbington, M. S. (2012). Probabilistic eruption forecasting at short and long time scales. *Bulletin of Volcanology*, 74(8):1777–1805.

Moretto, S., Bozzano, F., Esposito, C., and Mazzanti, P. (2016). Lesson learned from the pre-collapse time series of displacement of the Preonzo landslide (Switzerland). *Rendiconti Online della Societá Geologica Italiana*, 41:247 – 250.

Neri, A., Bevilacqua, A., Esposti Ongaro, T., Isaia, R., Aspinall, W. P., Bisson, M., Flandoli, F., Baxter, P. J., Bertagnini, A., Iannuzzi, E., Orsucci, S., Pistolesi, M., Rosi, M., and Vitale, S. (2015). Quantifying volcanic hazard at Campi Flegrei caldera (Italy) with uncertainty assessment: 2. Pyroclastic density current invasion maps. *Journal of Geophysical Research: Solid Earth*, 120(4):2330–2349.

Ortiz, R., Moreno, H., García, A., Fuentealba, G., Astiz, M., Pena, P., Sánchez, N., and Tárraga, M. (2003). Villarrica volcano (Chile): characteristics of the volcanic tremor and forecasting of small explosions by means of a material failure method. *Journal of Volcanology and Geothermal Research*, 128(1):247 – 259.

Richardson, J., Wilson, J., Connor, C., Bleacher, J., and Kiyosugi, K. (2017). Recurrence rate and magma effusion rate for the latest volcanism on Arsia Mons, Mars. *Earth and Planetary Science Letters*, 458:170–178.

Salvage, R. and Neuberg, J. (2016). Using a cross correlation technique to refine the accuracy of the Failure Forecast Method: Application to Soufriére Hills volcano, Montserrat. *Journal of Volcanology and Geothermal Research*, 324:118 – 133.

Salvage, R. O., Karl, S., and Neuberg, J. W. (2017). *Volcano Seismology: Detecting Unrest in Wiggly Lines*, pages 1–17. Springer Berlin Heidelberg, Berlin, Heidelberg.

Selva, J., Orsi, G., Di Vito, M. A., Marzocchi, W., and Sandri, L. (2012). Probability hazard map for future vent opening at the Campi Flegrei caldera, Italy. *Bulletin of Volcanology*, 74(2):497–510.

Smith, R. and Kilburn, C. (2010). Forecasting eruptions after long repose intervals from accelerating rates of rock fracture: The June 1991 eruption of Mount Pinatubo, Philippines. *Journal of Volcanology and Geothermal Research*, 191(1):129 – 136.

Smith, R., Sammonds, P. R., and Kilburn, C. R. (2009). Fracturing of volcanic systems: Experimental insights into pre-eruptive conditions. *Earth and Planetary Science Letters*, 280(1):211 – 219.

Sparks, R. and Aspinall, W. (2004). *Volcanic activity: frontiers and challenges in forecasting, prediction and risk assessment*, volume 19 of *Geophysical Monograph 150*, pages 359–373. IUGG.

Tadini, A., Bevilacqua, A., Neri, A., Cioni, R., Aspinall, W. P., Bisson, M., Isaia, R., Mazzarini, F., Valentine, G. A., Vitale, S., Baxter, P. J., Bertagnini, A., Cerminara, M., de Michieli Vitturi, M., Di Roberto, A., Engwell, S., Esposti Ongaro, T., Flandoli, F., and Pistolesi, M. (2017a). Assessing future vent opening locations at the Somma-Vesuvio volcanic complex: 2. Probability maps of the caldera for a future Plinian/sub-Plinian event with uncertainty quantification. *Journal of Geophysical Research: Solid Earth*, 122(6):4357–4376.

Tadini, A., Bisson, M., Neri, A., Cioni, R., Bevilacqua, A., and Aspinall, W. P. (2017b). Assessing future vent opening locations at the Somma-Vesuvio volcanic complex: 1. A new information geodatabase with uncertainty characterizations. *Journal of Geophysical Research: Solid Earth*, 122(6):4336–4356.

Tárraga, M., Carniel, R., Ortiz, R., Marrero, J. M., and García, A. (2006). On the predictability of volcano-tectonic events by low frequency seismic noise analysis at Teide-Pico Viejo volcanic complex, Canary Islands. *Natural Hazards and Earth System Science*, 6(3):365–376.

Vasseur, J., Wadsworth, F. B., Lavallée, Y., Bell, A. F., and Main, I. G. (2015). Heterogeneity: The key to failure forecasting. *Scientific Reports*, 453:13259 – 13265.

Voight, B. (1987). Phenomenological law enables accurate time forecasts of slope failure. In *Int. Soc. Rock Mechanics, 7th International Congress of Rock Mechanics, Montreal, Canada*.

Voight, B. (1988a). A method for prediction of volcanic eruptions. *Nature*, 332:125–130.

Voight, B. (1988b). Material science law applies to time forecasts of slope failure. In *5th International Symposium on Landslides, Lausanne, Switzerland*.

Voight, B. (1989). A relation to describe rate-dependent material failure. *Science*, 243(4888):200–203.

Voight, B. and Cornelius, R. R. (1991). Prospects for eruption prediction in near real-time. *Nature*, 350:695–698.

Voight, B., Orkan, N., and Young, K. (1989). Deformation and failure-time prediction in rock mechanics. In *Rock Mechanics as a Guide for Efficient Utilization of Natural Resources*.

Voight, B., Young, K., Hidayat, D., Subandrio, Purbawinata, M., Ratdomopurbo, A., Suharna, Panut, Sayudi, D., LaHusen, R., Marso, J., Murray, T., Dejean, M., Iguchi, M., and Ishihara, K. (2000). Deformation and seismic precursors to dome-collapse and fountain-collapse nuées ardentes at Merapi Volcano, Java, Indonesia, 1994-1998. *Journal of Volcanology and Geothermal Research*, 100(1):261 – 287.